nature materials

LETTERS

PUBLISHED ONLINE: 15 MAY 2011 | DOI: 10.1038/NMAT3020

Fast current-induced domain-wall motion controlled by the Rashba effect

Ioan Mihai Miron[1,2]*, Thomas Moore[1,3], Helga Szambolics[1], Liliana Daniela Buda-Prejbeanu[1], Stéphane Auffret[1], Bernard Rodmacq[1], Stefania Pizzini[3], Jan Vogel[3], Marlio Bonfim[4], Alain Schuhl[1,3] and Gilles Gaudin[1]

The propagation of magnetic domain walls induced by spin-polarized currents[1–5] has launched new concepts for memory and logic devices[6–8]. A wave of studies focusing on permalloy (NiFe) nanowires[9] has found evidence for high domain-wall velocities (100 m s^{-1}; refs 10,11), but has also exposed the drawbacks of this phenomenon for applications. Often the domain-wall displacements are not reproducible[12], their depinning from a thermally stable position is difficult[13] and the domain-wall structural instability (Walker breakdown[14,15]) limits the maximum velocity[10]. Here, we show that the combined action of spin-transfer and spin–orbit torques offers a comprehensive solution to these problems. In an ultrathin Co nanowire, integrated in a trilayer with structural inversion asymmetry (SIA), the high spin-torque efficiency[16] facilitates the depinning and leads to high mobility, while the SIA-mediated Rashba field[17–19] controlling the domain-wall chirality stabilizes the Bloch domain-wall structure. Thus, the high-mobility regime is extended to higher current densities, allowing domain-wall velocities up to 400 m s^{-1}.

Domain walls are local deformations of the magnetization at the boundary separating two uniformly and oppositely magnetized domains (Fig. 1). A magnetic field can favour the expansion of a domain over its neighbours and as a result shift the bordering domain walls. This process can take place by two distinct mechanisms. First, at low fields, the wall structure is slightly distorted, and an internal torque associated with this deformation propagates the wall. This mechanism leads to a regime of high domain-wall mobility. Above a critical field value, called Walker breakdown[14,15], a different regime of low domain-wall mobility ensues: the internal deformation is so strong that the wall structure is altered. As the magnetization inside the wall precesses around the applied field, the Bloch domain wall periodically changes its chirality by transiting through a Néel structure. The steady motion induced by the constant domain-wall deformation is replaced by back and forth motion associated with its continuous metamorphosis.

Unlike the field-induced domain-wall motion, the injection of an electric current produces unidirectional motion of domain walls through a more complex interaction. Its effect, generically called spin-transfer torque (STT), has two components (Fig. 1e,f). The first one (non-adiabatic) mimics an easy-axis magnetic field, whereas the second (adiabatic) acts as a hard-axis field always perpendicular to the magnetization inside the domain wall[3,5]. It is common to designate the deviation from adiabaticity of the STT by β, the ratio between the non-adiabatic and adiabatic torques.

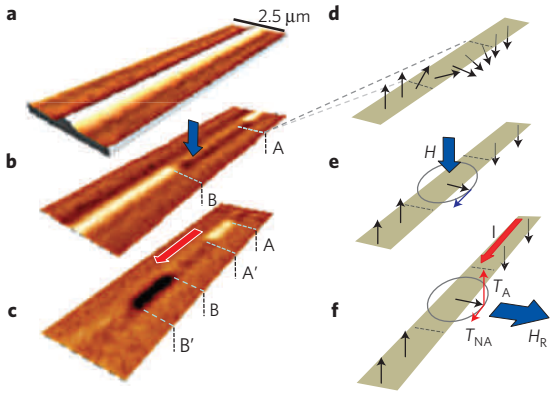

Figure 1 | Effects of magnetic field and electric current on domain walls. **a**, Optical micrograph of a Pt/Co/AlO$_x$ wire. To better distinguish from the magnetic contrast in the following images, the micrograph is given an artificial height profile. **b**, Differential Kerr microscopy image of the domain structure after application of a magnetic field (blue arrow). In the reference image (not shown) the magnetization points upwards. The magnetic field brings a domain wall from each end of the wire towards the middle, to positions A and B. The magnetic contrast from the reversed domains (which have magnetization pointing down) is bright. **c**, Under the effect of current (red arrow), the domain walls move in the same direction (from A to A′ and B to B′). As one of the domains previously created by field grows while the other shrinks, the differential image (**c**) contains both bright and dark contrast. **d**, Schematic representation of a domain wall. The black arrows symbolize the magnetization, continuously rotating between the two domains. **e**, Schematic representation of the torque created by an easy-axis magnetic field (thick blue arrow) on the domain wall. In a simplified domain-wall structure (a region of in-plane uniform magnetization) the torque (thin blue arrow) points in-plane, perpendicular to the magnetization. **f**, Instead of a single torque, the electric current produces two torques (red arrows). One points in-plane, similar to the field torque (T_{NA} non-adiabatic), whereas the other is perpendicular to the plane (T_A adiabatic). In our samples, besides producing STT, the current generates a strong in-plane Rashba effective field (H_R).

In spite of the relative complexity of the STT with respect to the simple field torque, the same domain-wall motion mechanisms are predicted[5]. Below the Walker breakdown, the steady domain-wall motion is controlled by the non-adiabatic torque, which together with the damping constant (α) dictates the velocity $v = \beta/\alpha \cdot u$.

[1]SPINTEC, UMR-8191, CEA/CNRS/UJF/GINP, INAC, F-38054 Grenoble, France, [2]Catalan Institute of Nanotechnology (ICN-CSIC), UAB Campus, E-08193 Barcelona, Spain, [3]Institut Néel, CNRS/UJF, B.P. 166, F-38042 Grenoble, France, [4]Departamento de Engenharia Elétrica, Universidade Federal do Paraná, Curitiba, Paraná, 81531-970, Brazil. *e-mail: mihai.miron.icn@uab.es.

Here, $u = j((P\mu_B g)/(2eM_S))$, where j is the current density, P is the current polarization, μ_B is the Bohr magneton, g is the Landé factor, e is the electron charge and M_S is the sample's saturation magnetization. Above the Walker breakdown, the adiabatic term dominates the turbulent domain-wall dynamics ($v = u$).

The usefulness of current-induced domain-wall motion for applications depends on two crucial parameters: the maximum domain-wall velocity and the critical current necessary to depin the domain wall, which determine the speed and power consumption of a device. Ideally, both of these characteristics could be optimized by engineering materials where the non-adiabaticity is very strong. A higher non-adiabatic (β) torque will simultaneously ease the depinning and increase the domain-wall mobility ($v = \beta/\alpha \cdot u$) to values larger than those given by the spin transfer. However, there is a contraindication for this recipe: increasing β shifts the position of the Walker breakdown ($\sim|1-\beta/\alpha|^{-1}$) to lower currents. Unless the Walker breakdown instability separating high- and low-mobility regimes can be prevented by alternative means, the advantages of increasing β are rapidly lost.

The numerous experiments on permalloy (NiFe) nanowires illustrate well such constraints on the current-induced domain-wall motion. Domain-wall depinning even from feeble traps requires relatively high threshold currents[2,13], indicating a rather inefficient STT (small β). On the other hand, in high-quality samples with weak pinning, domain walls can reach high velocities[10,11] because α is even smaller than β (ref. 9; high β/α). Nevertheless, as predicted by models[5], the Walker breakdown limits the maximum velocity[10,20]. As successful applications rely on fast and reproducible domain-wall displacements, experiments on NiFe identify the domain-wall depinning at low currents and the prevention of domain-wall transformations at the Walker breakdown as the main future challenges. Although these issues were separately addressed with some success in the past[21–24], a simple, unique solution to the problem is still missing[25]. For example, to improve the depinning, one approach was to use short current pulses (~1 ns) and resonantly excite the domain-wall oscillations inside its pinning potential[21]. This reduces the threshold current required for domain-wall motion, but the depinning probability oscillates with the pulse length, has a stochastic character and depends on the details of the pinning landscape. Concerning the second limitation, a promising method of delaying the Walker breakdown and enabling higher velocities is to apply a hard-axis magnetic field and thereby raise the energy barrier for domain-wall transformations[22,23]. However, applying an external field with the required intensity and spatial homogeneity is not a realistic solution for a device.

Here we show that the use of SIA layer structures such as Pt(3 nm)/Co(0.6 nm)/AlO_x(2 nm) offers an effective solution to these limitations. We have previously shown that the SIA leads to an important enhancement of the non-adiabatic spin torque ($\beta \approx 1$; ref. 16) and to the occurrence of an effective Rashba field[17] (H_R). Here, we demonstrate new domain-wall dynamics and establish the role of these two key parameters. Namely, owing to the large β ($\approx$1; ref. 16), the current exerts a high pressure on the domain wall, while H_R (refs 17,18) acting naturally along the hard axis stabilizes the Bloch configuration. The combination of high pressure and rigid structure yields domain-wall displacements that do not exhibit oscillating behaviour as in NiFe (ref. 21) or suffer the velocity decrease inherent to the Walker breakdown. On the contrary, subnanosecond current pulses induce reproducible domain-wall displacements at high velocity, an essential step towards viable devices.

Using a wide-field Kerr microscope we image the displacements induced by series of current pulses of varying length and amplitude in an array of 20 identical wires (500 nm width and 10 μm length; see Methods). Despite the high density of strong pinning centres often cited to prevent long-distance domain-wall motion in out-of-plane magnetized materials[26,27], we observe sustained domain-wall displacements in the direction of the electric current. For the long, low-density pulses, there is a large dispersion in the domain-wall displacements (important size distribution of dark and bright stripes in Fig. 2a) characteristic of thermally assisted depinning. On the contrary, for the short, intense pulses, the domain-wall motion is remarkably reproducible (Fig. 2b), indicating that as the current density increases the domain-wall motion is less influenced by thermal fluctuations.

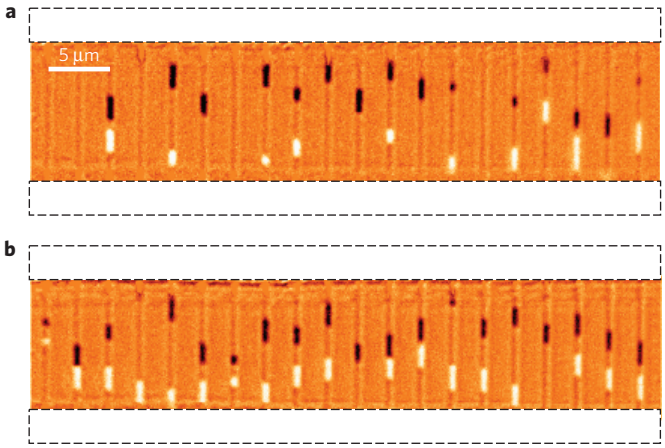

Figure 2 | Current-induced domain-wall displacements observed by Kerr microscopy. a,**b**, Differential Kerr micrographs showing the domain-wall displacements (stripes of dark/light contrast in the wires) induced by 20×3.0 ns current pulses of density 1.2×10^{12} A m^{-2} (**a**) and by 15×0.64 ns current pulses of density 2.6×10^{12} A m^{-2} (**b**). The wires are 500 nm wide and 10 μm long with a periodicity of 2.5 μm. The white rectangles symbolize the Au contact pads used to lower the device resistance. Note that in two of the wires in **b** (1 and 7 counting from the left), the dark and bright stripes are much shorter than in the other wires. Here this does not mean that the domain walls travel shorter distances. It occurs because initially the two domain walls in the wire were very close together, and the trailing domain wall overruns part of the trace left by the domain wall in front, undoing the contrast and reverting it to grey. The black and white spots actually indicate the position of a small domain before and after the pulse. In this case, the domain is translated over a distance much larger than its size.

The specific features of the domain-wall dynamics allowing the understanding of STT phenomena are usually concealed by domain-wall pinning to sample imperfections. Generally, theories treat perfect wires at 0 K, and do not include the effects of thermal activation associated with the depinning. Thus, to make a correct comparison to theory, separating the STT and thermal contributions to domain-wall motion is essential. To accumulate significant statistical data, able to reduce measurement fluctuations provoked by temperature and disorder, we average between 10^3 and 10^5 independent events. Repeating the experiment for at least three different pulse durations at each current density allows probing the variation of displacement versus pulse length. The resulting linear dependence (Fig. 3a) yields two important parameters: the slope determines the domain-wall velocity, and the intercept on the abscissa is an estimate of the average depinning time. As the current density increases, this waiting time decreases monotonically from values as large as 7 ns to saturation at 0.3 ± 0.1 ns (Supplementary Fig. S5). This implies that, for the longer, lower-density pulses, the delay is determined mainly by thermal activation, whereas for the shorter, higher-density pulses, the thermally activated regime is bypassed, and the depinning is delayed only by the finite rise time of the pulse (~0.25 ns).

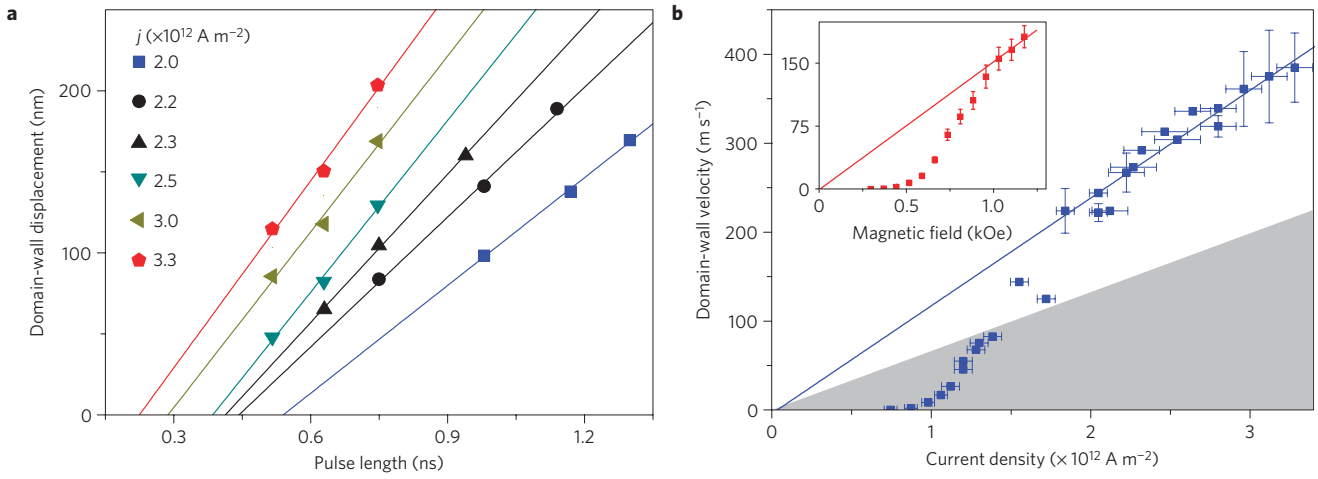

Figure 3 | Domain-wall velocity induced by current or field in the PtCoAlO$_x$ layers. a, Current-induced domain-wall displacement as a function of pulse length, for current densities j ranging from 2.0 to 3.3 × 10^{12} A m^{-2}. Each data point is an average over more than 10^3 individual displacements. Error bars calculated as the standard error of the average value are smaller than the data points. **b**, Domain-wall velocity as a function of the current density. Vertical error bars are calculated as the error of the linear regression. Horizontal error bars are important only for the shortest pulses where the plateau of constant current is reduced. They are caused by the imprecision in the determination of the pulse height. The solid line is a linear fit to the domain-wall flow regime (occurring for $j > 1.8 \times 10^{12}$ A m^{-2}). The shaded area maps the region where the velocity values are compatible with the turbulent motion. The inset shows a measurement of the domain-wall velocity as a function of the magnetic field. When $H > 1.0$ kOe, the domain-wall mobility saturates (indicated by the red solid line) and thus demonstrates a similar behaviour to the current-induced velocity.

Figure 3b shows the domain-wall velocity plotted as a function of current density. Similarly to the creep and flow regimes seen in studies of field-driven motion[26], the domain-wall mobility increases at low currents and saturates at higher values ($\sim 1.8 \times 10^{12}$ A m^{-2}). Moreover, we observe that the onset of the constant-mobility regime coincides with the saturation of the delay time (Supplementary Fig. S5). This proves that for the high current densities the velocity determination is not affected by pinning, allowing the comparison of experimental results to values predicted by theory.

An outstanding feature of this comparison (Fig. 3b) is that even in the limit of full current polarization ($P = 1$), the measured domain-wall mobility exceeds by a factor of 2 the value expected in the turbulent-motion regime ($v = u$). Besides the value of the saturation magnetization ($\mu_0 M_S \approx 1$ T; ref. 17), u depends only on physical constants; therefore, such high mobility can be explained only by considering the β/α correction factor ensuing from the steady domain-wall motion ($v = \beta/\alpha \cdot u$). As this analysis rules out the scenario of turbulent motion, we conclude that in the range of currents used experimentally the domain wall translates steadily under the effect of the non-adiabatic torque.

To further prove this point, we exploit the most distinctive feature of non-adiabatic STT: its effects are identical to those of an easy-axis magnetic field. Employing an established method[26], we measure the field-induced domain-wall displacement in an unpatterned film and compare it with the current-induced behaviour. Again, we find that at first the mobility increases but eventually saturates (Fig. 3b, inset). As constant-mobility regimes, independent of pinning, are observed for both current- and field-driven domain-wall motion, we can compare their respective velocity values and determine a field–current correspondence. We find within experimental error that this conversion factor (0.1 T corresponding to 1.25×10^{12} A m^{-2}) is the same as the one previously observed by quasi-static measurements at lower current density (far below the Walker breakdown) on the same system[16]. The extension of the same field–current equivalence up to the highest current densities proves that the same physical mechanism governs the domain-wall motion. Relying on simple comparison of direct measurements, this method circumvents any potential imprecision in the values of physical quantities used for estimations and confirms that domain-wall motion is indeed in the steady-flow regime.

To explain why the Walker breakdown is never observed, we consider the effects of the H_R on the domain-wall dynamics. As it points in-plane, perpendicular to the wire direction, H_R will favour one of the two possible chiralities of the domain-wall Bloch structure. As the domain-wall transformations above the Walker breakdown involve the periodic reversal of the chirality, the asymmetry induced by H_R obstructs these cyclic transformations and maintains the high-mobility regime.

If this scenario is correct, and indeed the H_R lifts the chiral degeneracy, a second phenomenon should also occur. When the chirality is initially selected to oppose H_R, the application of a current pulse should switch it to the state favoured by H_R (Fig. 4a). Similarly to the turbulent regime where the chirality changes repeatedly, this single reversal is also expected to influence the domain-wall motion[28]. Therefore, its occurrence should be detectable by simple measurements of domain-wall displacements.

To probe this effect we slightly adjust our experiment: before applying each current pulse (from a series of 10) we set the domain-wall chirality using an external in-plane magnetic field perpendicular to the wire (see Methods). The resulting displacements, shown in Fig. 4b, are clearly smaller when the initial chirality is opposing H_R, indicating that the chirality has indeed switched. If we then repeat the experiment, but without using any external field, we find that the displacements are identical to those obtained when the chirality was prepared parallel to H_R. This is expected as after the first pulse the domain-wall chirality is set along H_R whatever its initial state, and then maintained throughout the nine remaining pulses. This evidence of the chirality dependence of the displacements is additional confirmation of the steady domain-wall motion.

An in-depth micromagnetic analysis is presented in the Supplementary Information. Offering detailed insight into the domain-wall dynamics within different scenarios, the comparison between micromagnetic predictions and measurements confirms the influence of H_R on the domain-wall chirality together with its consequences on the displacement values. As an example, we show in Fig. 4c the results of the micromagnetic simulations for

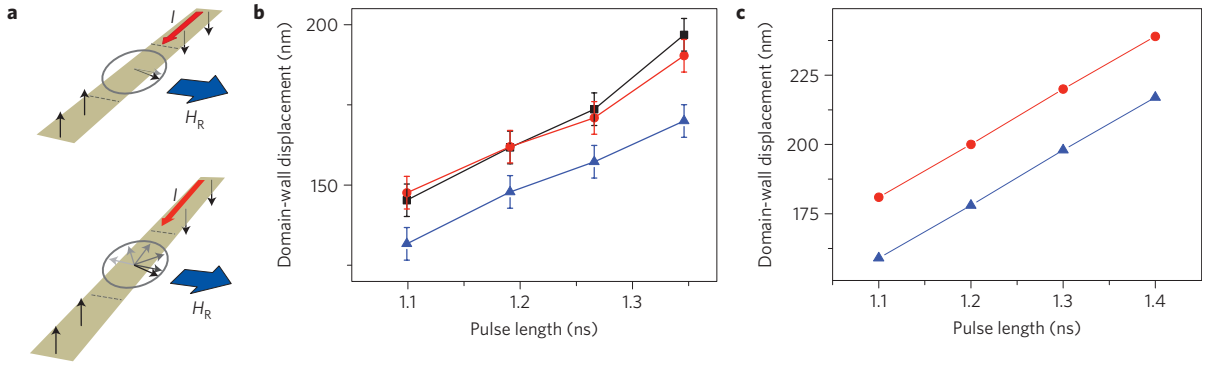

Figure 4 | Domain-wall chirality reversal induced by H_R. a, Schematic representation of the effect of H_R on the domain-wall chirality. If they are initially parallel, the domain-wall distortion is limited by H_R. When opposed, the chirality is switched once, and then, similarly to the previous case, maintained. **b**, Measurements of domain-wall displacements for a current density fixed at 1.4×10^{12} A m^{-2} for different directions of the external field used to set the domain-wall chirality: in red the external field of 1.3 kOe points in the same direction as the Rashba field, in blue it opposes the Rashba field, and in black, no external field is applied. Compared with the previous case, the error bars are larger owing to the smaller number of counts limited by the longer duration of the experiment. **c**, Micromagnetic simulations reproduce the experimental result. When the chirality is opposed to H_R (blue curve) the displacement is smaller.

the chirality reversal induced by the H_R. As these simulations use parameters previously determined on the same system, it is not surprising that the value of the domain-wall velocity (the slope of the dependence) and the correction to the displacement induced by the chirality reversal (the downward shift of the blue curve) are accurately reproduced. The only noticeable imprecision, the overestimation of the delay time, is due to the absence of the pinning in simulations.

On the basis of the conclusion that, owing to the stabilizing effect of H_R, the non-adiabatic STT is the sole driver of the current-induced domain-wall motion, we can now anticipate further improvements. By engineering the SIA in materials with low damping (for example, CoNi with $\alpha \approx 0.03$; ref. 29) to obtain $\beta \sim 1$ and a similarly large H_R, an especially favourable situation for domain-wall motion may result. The high β would facilitate depinning, the large β/α would give an increased mobility while H_R would prevent Walker breakdown. In such a case we estimate that domain-wall velocities could reach up to 10 km s^{-1} for current densities of the order of 10^{12} A m^{-2}.

Methods

To study current-induced domain-wall motion in Pt/Co/AlO$_x$, wires of 500 nm width and 10 μm length were patterned in sets of 20 by electron-beam lithography and Ar ion etching of magnetron sputtered films. Low-resistance Au pads were positioned at the ends of each wire array using optical lithography, and domain walls were prepared in the wires by applying an external out-of-plane magnetic field. The domain-wall displacements induced by current pulses of varying length (full-width at half-maximum 0.5–11.5 ns) and amplitude ($j = 0.7$–3.3×10^{12} A m^{-2}) were then monitored by a commercial wide-field Kerr microscope. To visualize the effect of the current, a magnetic image made before the pulse injection was subtracted from an image taken afterwards (Fig. 1). As the current induces domain-wall motion simultaneously in every wire, and one wire could contain two domain walls, a single image could give information about as many as 40 domain walls. The current pulses were recorded on an oscilloscope connected in series with the sample. Values of the domain-wall displacements were determined by averaging all individual displacements observed on up to 10 images made under the same conditions of pulse length and amplitude.

To obtain domain-wall displacements on the micrometre scale, the pulses were repeated between 6 and 10,000 times, depending on the current density. The time between the end of one pulse and the beginning of the next was of the order of milliseconds to separate the effects of consecutive pulses. A further increase of the time between the pulses did not influence the overall domain-wall displacement, demonstrating that this time is long enough for the wires to evacuate the heat produced during the pulse. When increasing the number of pulses n for a given j, we observed a linear increase of the domain-wall displacement, and because the pulses are well separated in time, we concluded that their effect on the domain-wall motion is cumulative. Consequently, the displacement corresponding to a single pulse may be obtained by dividing the total observed displacement by n.

The field necessary for the reversal of the domain-wall chirality is upper-bounded at the value of its anisotropy field: the static in-plane field necessary to transform the Bloch wall into a Néel wall. From domain-wall shape considerations (the ratio between the thickness of the wire (0.5 nm) and the width of the domain wall (4.2 nm)), we estimate this field to be no larger than 1 kOe. To set the domain-wall chirality, a magnetic field of 1.3 kOe was continuously applied for 1 s. A current pulse of 1.4×10^{12} A m^{-2} was applied 4 s after the removal of the magnetic field. To obtain visible domain-wall displacements, this sequence was repeated 10 times. When measuring the displacement in the absence of magnetic field, the separation between the 10 current pulses remained at 5 s. Note that this chirality experiment was carried out on a sample patterned from a different wafer. This explains why the displacements are slightly different from the previous ones. We believe that this difference is mainly caused by different domain-wall pinning, because the value of the domain-wall mobility (170 m s^{-1} at 1.4×10^{12} A m^{-2}) corresponds to the flow regime observed in the first sample. The very short delay time (0.25 ns) is also consistent with this scenario.

Received 14 December 2010; accepted 30 March 2011; published online 15 May 2011

References

1. Vernier, N., Allwood, D. A., Atkinson, D., Cooke, M. D. & Cowburn, R. P. Domain wall propagation in magnetic nanowires by spin-polarized current injection. *Europhys. Lett.* **65,** 526–532 (2004).
2. Yamaguchi, A. *et al.* Real-space observation of current-driven domain wall motion in submicron magnetic wires. *Phys. Rev. Lett.* **92,** 077205 (2004).
3. Zhang, S. & Li, Z. Roles of nonequilibrium conduction electrons on the magnetization dynamics of ferromagnets. *Phys. Rev. Lett.* **93,** 127204 (2004).
4. Tatara, G. & Kohno, H. Theory of current-driven domain wall motion: Spin transfer versus momentum transfer. *Phys. Rev. Lett.* **92,** 086601 (2004).
5. Thiaville, A., Nakatani, Y., Miltat, J. & Suzuki, Y. Micromagnetic understanding of current-driven domain wall motion in patterned nanowires. *Europhys. Lett.* **69,** 990–996 (2005).
6. Parkin, S. S. P., Hayashi, M. & Thomas, L. Magnetic domain-wall racetrack memory. *Science* **320,** 190–194 (2008).
7. Hayashi, M., Thomas, L., Moriya, R., Rettner, C. & Parkin, S. S. P. Current-controlled magnetic domain-wall nanowire shift register. *Science* **320,** 209–211 (2008).
8. Allwood, D. A. *et al.* Magnetic domain-wall logic. *Science* **309,** 1688–1692 (2005).
9. Beach, G. S. D., Tsoi, M. & Erskine, J. L. Current-induced domain wall motion. *J. Magn. Magn. Mater.* **320,** 1272–1281 (2008).
10. Hayashi, M. *et al.* Current driven domain wall velocities exceeding the spin angular momentum transfer rate in permalloy nanowires. *Phys. Rev. Lett.* **98,** 037204 (2007).
11. Meier, G. *et al.* Direct imaging of stochastic domain-wall motion driven by nanosecond current pulses. *Phys. Rev. Lett.* **98,** 187202 (2007).
12. Kläui, M. *et al.* Direct observation of domain-wall configurations transformed by spin currents. *Phys. Rev. Lett.* **95,** 026601 (2005).
13. Hayashi, M. *et al.* Dependence of current and field driven depinning of domain walls on their structure and chirality in permalloy nanowires. *Phys. Rev. Lett.* **97,** 207205 (2006).

14. Beach, G. S. D., Nistor, C., Knutson, C., Tsoi, M. & Erskine, J. L. Dynamics of field-driven domain-wall propagation in ferromagnetic nanowires. *Nature Mater.* **4,** 741–744 (2005).
15. Schryer, N. L. & Walker, L. R. The motion of 180° domain walls in uniform dc magnetic fields. *J. Appl. Phys.* **45,** 5406–5420 (1974).
16. Miron, I. M. *et al.* Domain wall spin torquemeter. *Phys. Rev. Lett.* **102,** 137202 (2009).
17. Miron, I. M. *et al.* Current-driven spin torque induced by the Rashba effect in a ferromagnetic metal layer. *Nature Mater.* **9,** 230–234 (2010).
18. Manchon, A. & Zhang, S. Theory of nonequilibrium intrinsic spin torque in a single nanomagnet. *Phys. Rev. B* **78,** 212405 (2008).
19. Pi, U. H. *et al.* Tilting of the spin orientation induced by Rashba effect in ferromagnetic metal layer. *Appl. Phys. Lett.* **97,** 162507 (2010).
20. Moore, T. A. *et al.* Scaling of spin relaxation and angular momentum dissipation in permalloy nanowires. *Phys. Rev. B* **80,** 132403 (2009).
21. Thomas, L. *et al.* Oscillatory dependence of current-driven magnetic domain wall motion on current pulse length. *Nature* **443,** 197–200 (2006).
22. Bryan, M. T., Schrefl, T., Atkinson, D. & Allwood, D. A. Magnetic domain wall propagation in nanowires under transverse magnetic fields. *J. Appl. Phys.* **103,** 073906 (2008).
23. Kunz, A. & Reiff, S. C. Fast domain wall motion in nanostripes with out-of-plane fields. *Appl. Phys. Lett.* **93,** 082503 (2008).
24. Lewis, E. R. *et al.* Fast domain wall motion in magnetic comb structures. *Nature Mater.* **9,** 980–983 (2010).
25. Beach, G. Spintronics: Beyond the speed limit. *Nature Mater.* **9,** 959–960 (2010).
26. Metaxas, P. J. *et al.* Creep and flow regimes of magnetic domain-wall motion in ultrathin Pt/Co/Pt films with perpendicular anisotropy. *Phys. Rev. Lett.* **99,** 217208 (2007).
27. Burrowes, C. *et al.* Role of pinning in current driven domain wall motion in wires with perpendicular anisotropy. *Appl. Phys. Lett.* **93,** 172513 (2008).
28. Obata, K. & Tatara, G. Current-induced domain wall motion in Rashba spin–orbit system. *Phys. Rev. B* **77,** 214429 (2008).
29. Beaujour, J. M. L. *et al.* Ferromagnetic resonance study of sputtered CoNi multilayers. *Eur. Phys. J. B* **59,** 475–483 (2007).

Acknowledgements

We thank P. Gambardella for critically reading the manuscript and useful discussions. This work was partially supported by the ANR-07-NANO-034 'Dynawall' project and ERC (StG 203239). Samples were patterned at the NANOFAB facility of the Institut Néel (CNRS). The micromagnetic simulations were carried out using the Gilbert–Landau Fast Fourier Transform code initially developed by J.C. Toussaint.

Author contributions

I.M.M., T.M., A.S. and G.G. designed the experiment; I.M.M., G.G., S.A. and B.R. fabricated the samples. I.M.M. and T.M. carried out the experiments assisted by S.P., J.V., M.B. and G.G; I.M.M., T.M. and G.G analysed the data and wrote the manuscript; H.S. and L.D.B-P. carried out the micromagnetic simulations. All authors discussed the results and commented on the manuscript.

Additional information

The authors declare no competing financial interests. Supplementary information accompanies this paper on www.nature.com/naturematerials. Reprints and permissions information is available online at http://www.nature.com/reprints. Correspondence and requests for materials should be addressed to I.M.M.